International Journal of Minerals, Metallurgy and Materials
Volume 25, Number 9, September 2018, Page 1060
https://doi.org/10.1007/s12613-018-1657-9

Microstructure, mechanical properties, and wear resistance of VC_p-reinforced Fe-matrix composites treated by Q&P process

Ping-hu Chen[1,2], *Yi-bo Li*[1,2,3], *Rui-qing Li*[2,3], *Ri-peng Jiang*[3], *Song-sheng Zeng*[4], *and Xiao-qian Li*[1,2,3]

1) College of Mechanical and Electrical Engineering, Central South University, Changsha 410083, China
2) State Key Laboratory of High Performance Complex Manufacturing, Changsha 410083, China
3) Light Alloy Research Institutes, Central South University, Changsha 410083, China
4) Valin ArcelorMittal Automotive Steel Co., Ltd., Loudi 417000, China
(Received: 10 January 2018; revised: 4 April 2018; accepted: 13 April 2018)

Abstract: A quenching and partitioning (Q&P) process was applied to vanadium carbide particle (VCp)-reinforced Fe-matrix composites (VC-Fe-MCs) to obtain a multiphase microstructure comprising VC, V_8C_7, M_3C, α-Fe, and γ-Fe. The effects of the austenitizing temperature and the quenching temperature on the microstructure, mechanical properties, and wear resistance of the VC-Fe-MCs were studied. The results show that the size of the carbide became coarse and that the shape of some particles began to transform from diffused graininess into a chrysanthemum-shaped structure with increasing austenitizing temperature. The microhardness decreased with increasing austenitizing temperature but substantially increased after wear testing compared with the microhardness before wear testing; the microhardness values improved by 20.0% ± 2.5%. Retained austenite enhanced the impact toughness and promoted the transformation-induced plasticity (TRIP) effect to improve wear resistance under certain load conditions.

Keywords: vanadium carbide; Fe-matrix composites; quenching and partitioning process; transformation-induced plasticity effect; microhardness; impact toughness; wear resistance

1. Introduction

Vanadium carbide [1] has advantages of high hardness, excellent high-temperature strength, good corrosion resistance, and high chemical and thermal stability even at high temperatures [2–4]; therefore, it is widely used in industrial applications [5–7]. Vanadium carbide in alloys such as austenite/martensite steel and cast iron is formed by chemical reaction at temperatures ranging from 1100 to 1500°C [2,8–9], which improves the mechanical properties and wear resistance of composites reinforced with vanadium carbide. Furthermore, the mechanical properties and wear resistance of vanadium carbide-reinforced composites are greatly enhanced through optimization of the composition ratios of the carbon and vanadium elements and through application of a heat treatment to regulate the type and size of the microstructure [10–15], thereby extending the service life of the composites [16].

The quenching and partitioning (Q&P) process was first proposed by J. G. Speer in 2006. Plasticity and toughness can be improved through this process, which utilizes a carbon partition to stabilize austenite [17–18]. The Q&P process has been adopted to adjust the ratio of austenite in the matrix to enhance the mechanical properties and wear behavior of high-strength steels. A hardening layer of the Q&P-treated specimen can form during wear tests because of the transformation-induced plasticity (TRIP) effect [19–24]. The optimized Q&P process and its TRIP effect are beneficial to enhancing the mechanical properties and wear resistance of the materials. Therefore, these new vanadium carbide-reinforced Fe-matrix composites (VC-Fe-MCs) can replace high-chromium and high-manganese wear-resistant cast iron in some industries. However, the study of VC-Fe-MCs on its properties has been reported rarely.

In the present paper, the setting of austenitizing temperature and quenching temperature was optimized to enhance

Corresponding authors: Yi-bo Li E-mail: yibo.li@csu.edu.cn; Song-sheng Zeng E-mail: zsscsu@sina.com

the mechanical properties and wear resistance of VC-Fe-MCs to promote the application. The effects of heat-treatment parameters on the microstructures, mechanical properties, and wear resistance of VC-Fe-MCs were studied, and the TRIP effect before and after wear test was discussed.

2. Experimental

2.1. Materials and sample preparation

The chemical composition of the VC-Fe-MCs is listed in Table 1. The preparation process of VC-Fe-MCs is as follows. Firstly, ferrous scrap was melted in a 200-kg medium-frequency induction furnace. Secondly, to increase the absorptivity of vanadium, ferrovanadium was added into liquid iron after being deoxidized. Thirdly, a certain amount of pure titanium was added to accelerate the nucleation of vanadium carbide, after which the melted iron was deoxidized. The final de-oxidation was conducted by adding 0.5wt% pure aluminum. Finally, the liquid cast iron was poured into a sand mold at approximately 1450°C and then formed by cooling in air. A schematic of the pouring process has been reported elsewhere [25]. The size of ingots were 200 mm × 100 mm × 14 mm. Samples for microhardness tests, impact tests, and wear tests were cut to small ingots with volume of 10 mm × 10 mm × 10 mm , 10 mm × 10 mm × 55 mm, and 10 mm × 10 mm × 40 mm, respectively. All samples were prepared for a batch of VC-Fe-MCs ingots.

Table 1. Chemical composition of VC-Fe-MCs wt%

C	Si	Mn	V	Cr	Mo	Fe
2.80	1.5	3.0	8.1	2.0	1.5	Bal.

2.2. Heat-treatment technique

Heat treatments were carried out using a heat-treatment furnace. The heat-treatment schedules were based on the Q&P process and the TRIP effect. Specimens were austenitized at 900, 950, 1000, and 1050°C for 30 min and then quenched in a salt-bath furnace (55vol% KNO_3 + 45vol% $NaNO_2$ with a melting point of 130°C and service temperature range from 150 to 500°C) at 150, 180, 210, and 300°C respectively for several minutes before being partitioned at 320°C for 30 min and cooled to room temperature.

2.3. Measurement of mechanical properties and wear resistance

Material impact tests were carried out on a JBW-300B pendulum-type impact-testing machine with an impact energy of 150 J. Specimens were prepared without a notch. Each group included three specimens; the final reported value was an average of the results of the three specimens. The microhardness of the specimens before and after wear test was measured on a Zwick Roell Indentec Vickers tester (ZHV1-AFC, Germany) with a load of 9.8 N for a dwell time of 15 s. Five points were measured for every specimen, with the reported value being the average of the five values. A wear resistance test was performed using a block-on-cylinder-type wear testing machine (M-2000) at room temperature with a load of 200 N at a rotating speed of 400 r/min. The material of the cylinder was YG8 hard alloy with a hardness of HRA 89 and outer and inner diameters of 40 mm and 16 mm, respectively. The weight loss (mg) of the wear specimens was measured using an analytical balance, and the width and depth of the wear trace were measured by a reading microscope (JC10, China) and an ultra-deep field 3D microscope (VHX5000, Japan), which provided a quantitative correlation among weight loss, wear width, wear depth, and wear time.

2.4. Morphology characterization and composition analysis

The microstructure of the specimens was characterized by scanning electron microscopy (SEM) on a TESCAN MIRA 3 LMH/LMU electron microscope operated at 15–25 kV. The samples were examined before and after they were etched with a 4vol% nitric acid alcohol solution for 30 s. The fracture morphology of specimens after the impact test was characterized by SEM. The chemical composition of the specimens was analyzed by energy-dispersive spectroscopy (EDS). Phase identification of the samples was carried out using X-ray diffraction (XRD) with a Cu K_α radiation; the samples were scanned at a rate of 0.04°/s over the 2θ interval from 10 to 90°.

3. Results

3.1. Microstructures and XRD analysis

Fig. 1 displays the microstructure and composition analysis of an as-cast specimen. The microstructure was characterized by VC, V_8C_7, M_3C, pearlite, and a small amount of martensite. The size of VC was between 5 μm and 10 μm, and a small amount of V_8C_7 was observed as long strips. On the basis of XRD composition analysis (Fig. 1(b)), the carbide phases were identified as VC and V_8C_7. The crystal structure of VC was a 2 × 2 × 2 super cell of VC with 32 vanadium atoms and 32 carbon atoms. The crystal structure of V_8C_7 was the unit cell of V_8C_7 with 32 vanadium atoms

and 28 carbon atoms [26]; the microstructure is shown in Fig. 1(c) and Fig. 1(d). α-Fe in the matrix was mainly pearlite with a small amount of martensite. The microstructure is shown in Fig. 1(d).

Fig. 2 shows the XRD composition analysis of the VC-Fe-MCs specimens austenitized at different temperatures and quenched at different temperatures. Compared with the XRD composition analysis of the as-cast specimen, it can be found that different proportions of the γ-Fe phase (retained austenite) were detected by XRD at different austenitizing

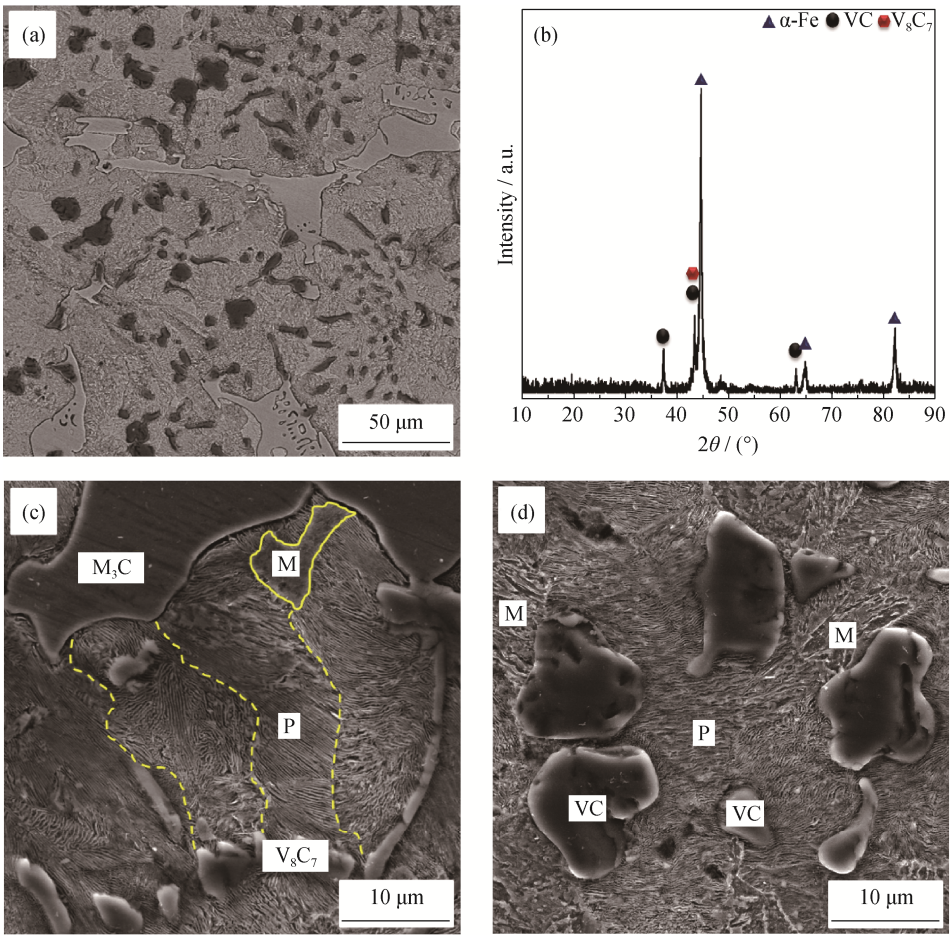

Fig. 1. Microstructure and XRD pattern of the as-cast specimen: (a) morphology and distribution of carbides; (b) XRD composition analysis; (c) and (d) M_3C, V_8C_7, VC, pearlite, and small amount of martensite.

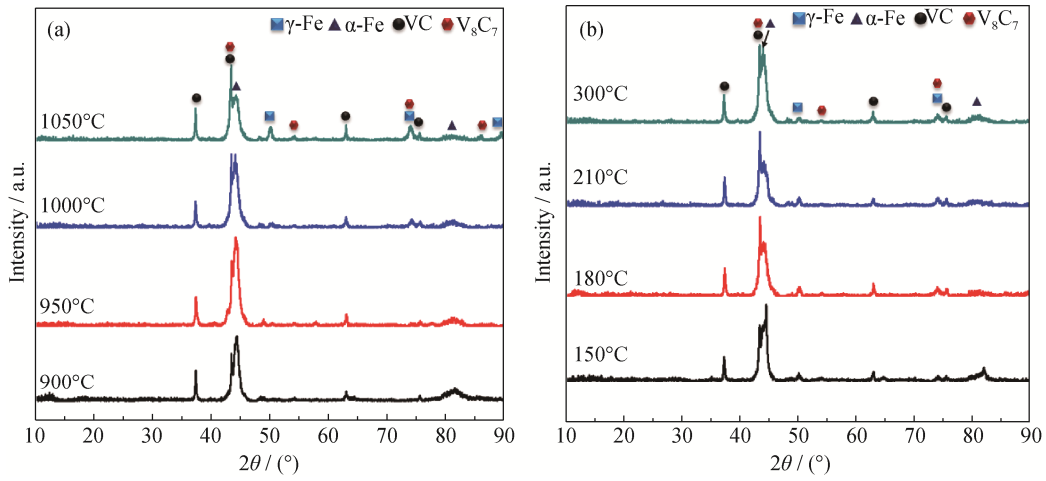

Fig. 2. XRD composition analysis of VC-Fe-MCs under different (a) austenitizing temperatures and (b) quenching temperatures.

temperatures and quenching temperatures. As shown in Fig. 2(a), the peaks associated with the γ-Fe phase (retained austenite) at 50, 75, and 90° increased in intensity, nevertheless, the peaks associated with the α-Fe phase at 45 and 82° decreased in intensity. The intensity of the VC peaks increased with increasing austenitizing temperature; however, with increasing quenching temperatures, the peak intensity of VC increased after initially decreasing, as shown in Fig. 2(b).

3.2. Microhardness and toughness

The effect of austenitizing temperature on impact toughness is shown in Fig. 3(a). The impact toughness initially increased and then decreased, reaching a toughness value greater than the initial value; the maximum value was 10.18 J/cm^2 at an austenitizing temperature of 1000°C. The effect of quenching temperature on impact toughness is shown in Fig. 3(b). Impact toughness increased with increasing quenching temperature. Fig. 4 shows the microhardness of specimens austenitized and quenched under different temperatures before and after wear test. The microhardness of the as-cast specimen was HRC 53.1 before and after wear test, whereas the microhardness of specimens changed substantially as the austenitizing and quenching temperatures were varied. Specifically, the microhardness decreased with increasing austenitizing temperature. As displayed in Fig. 4(a), the microhardness of specimens at austenitizing temperatures of 1000°C and 1050°C were lower than that of the as-cast specimens before wear test, which were HRC 50.3 and HRC 43.3, respectively. However, after carrying out continuous wear test for 60 min, the values increased by 17.3% and 40.9%, respectively. Fig. 4(b) shows the microhardness at different quenching temperatures before and after wear test. Before wear test, the microhardness of all the specimens was between HRC 47.5 and HRC 50.5. The microhardness increased substantially after wear test compared with that before test, and the hardness values improved by 20.0% ± 2.5%.

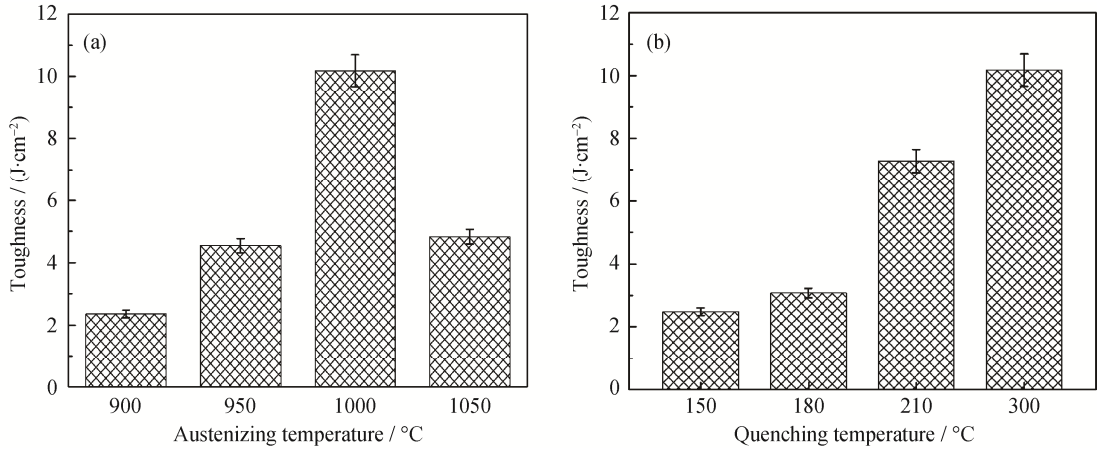

Fig. 3. Variation in toughness under different (a) austenitizing temperatures and (b) quenching temperatures.

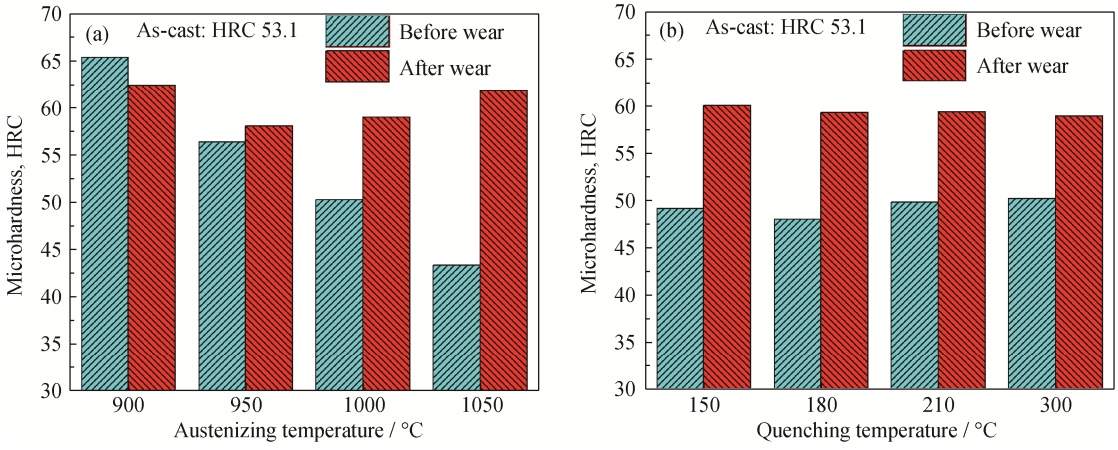

Fig. 4. Variation in microhardness under different (a) austenitizing and (b) quenching temperatures before and after wear testing.

3.3. Wear properties

Fig. 5(a) shows the weight losses at different austenitizing temperatures. In general, weight loss increased with wear time, and a comparison of the results of the wear experiment show that the wear loss of the specimen austenitized at 900°C was lower than the others; the maximum value was only 8.7 mg, whereas that of the as-cast specimen was 16.4 mg after wear for 60 min. The wear loss Δm at different austenitizing temperatures decreased in the order of $\Delta m_{AC} > \Delta m_{950} > \Delta m_{1000} > \Delta m_{1050} > \Delta m_{900}$, as shown in Fig. 5(a) (Δm_{AC} is a wear loss of the as-cast specimen). The effect of quenching temperature on wear loss was shown in Fig. 5(b), which indicated that little difference exists in wear losses at different quenching temperatures. After a wear time of 60 min, the wear loss of the specimen treated at 300°C ranked behind only that of the as-cast specimen. The wear losses of the specimens treated at 150–210°C were virtually equal. The wear width of the austenitized specimens was shown in

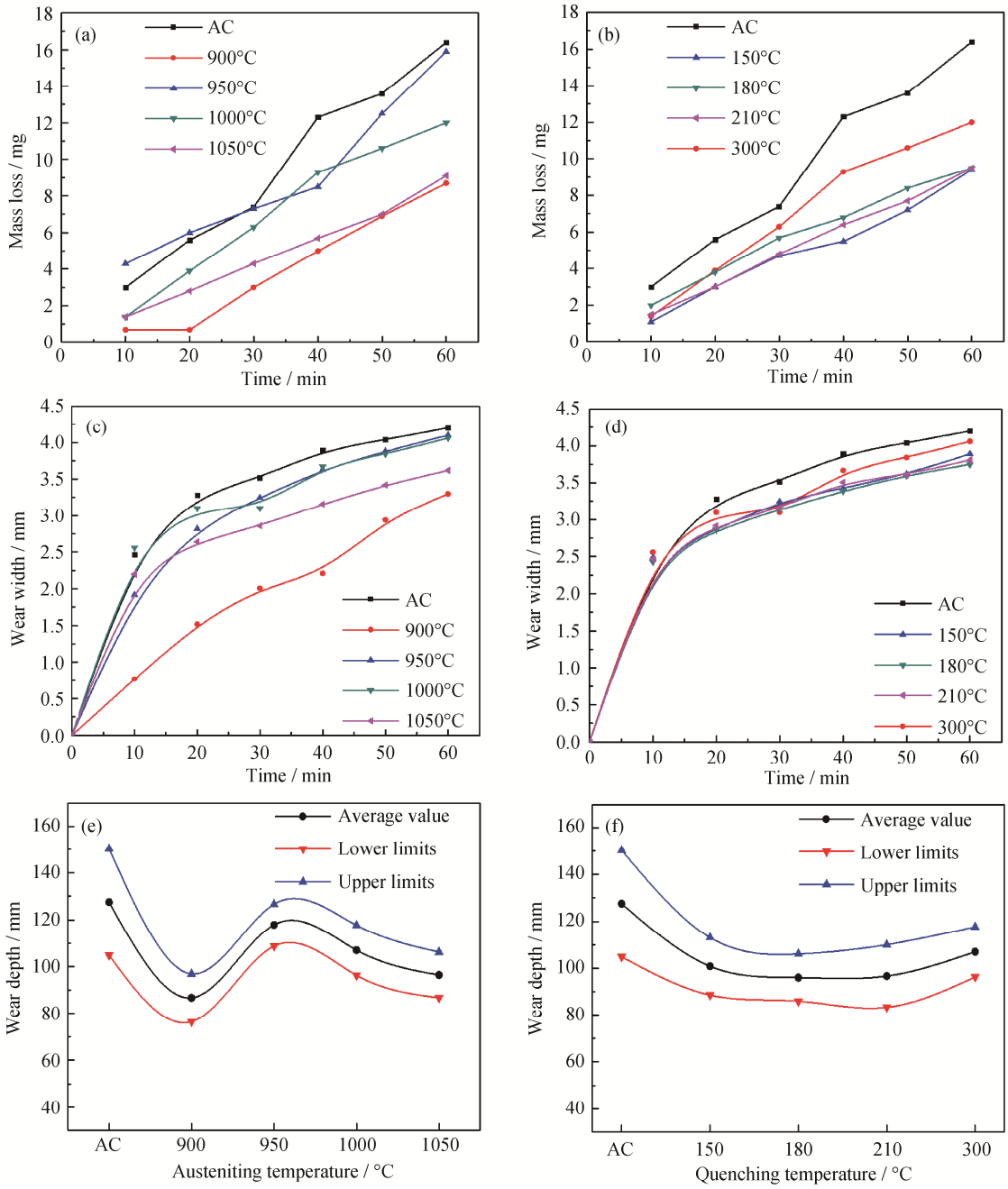

Fig. 5. Variation in weight losses under different (a) austenitizing temperatures and (b) quenching temperatures; variation in widths under different (c) austenitizing temperatures and (d) quenching temperatures; and variation in depths under different (e) austenitizing temperatures and (f) quenching temperatures. AC represents the as-cast specimen.

Fig. 5(c). The wear width exhibited a parabolic increase with wear time; however, the wear width of the 900°C-treated specimen exhibited linear growth. After a wear time of 60 min, the relationship of wear width agreed with that of wear loss. The maximum wear width of the as-cast specimen was 4.2 mm, and that of the specimen treated at 900°C exhibited a maximum value of 3.3 mm. The wear width exhibited a parabolic trend increase with increasing wear time when the quenching temperature was between 150°C and 300°C, as shown in Fig. 5(d). The maximum wear width of the specimens quenched at 180°C was the lowest (about 3.75 mm). The effect of the austenitizing temperature and quenching temperature on wear depth was shown in Fig. 5(e) and Fig. 5(f). The depth of the as-cast specimen was the largest, with an average value of 130 μm and a maximum value greater than 150 μm, as shown in Fig. 5(e). With an increase in austenitizing temperature, the wear depth increased after initially decreasing, whereas the wear depth of the specimen treated at 950° reached the maximum value. As shown in Fig. 5(f), in contrast, the wear-depth trend decreased initially and then increased.

4. Discussion

4.1. Effect of heat treatment on mechanical properties

On the basis of the experimental results, the impact toughness of the 900°C/300°C-treated specimen (where 900°C and 300°C are the austenitizing and quenching temperatures, respectively) was the lowest among the investigated samples, whereas that for the 1000°C/300°C-treated specimen was the highest. As shown in Fig. 6, four fracture morphologies were observed in the fracture surface of the 900°C/300°C-treated specimen: zone I (spalling of spherical carbides), zone II (brittle fracture of dendritic carbide), zone III (ductile fracture of Fe-matrix), and zone IV (brittle fracture of Fe-matrix). Carbides were mainly distributed in the ductile fracture region (zone III). The size of the spherical carbide particles was between 5 μm and 10 μm, whereas the dendritic carbides were larger than 250 μm, as shown in Fig. 6(a) and Fig. 6(b). The bonding between the spherical carbide and the Fe-matrix was poor, and a gap was readily apparent in the impact fracture. Cracks initiated in zone I under the impact condition. The bonding between the dendritic carbide and the Fe-matrix was quite good. The interdiffusion of alloying elements was detected between the dendritic carbide and the Fe- matrix, as shown in Fig. 6(c). However, the dendritic carbide was considered a ceramic particle, and brittle fracture occurred in zone II because the crack diffused from zone I to zone II (i.e., dendritic carbide). In addition, according to the mass fraction of the carbon element in the designed materials, the VC-Fe-MCs belong to particle reinforced wear-resistant cast iron, which exhibited poor

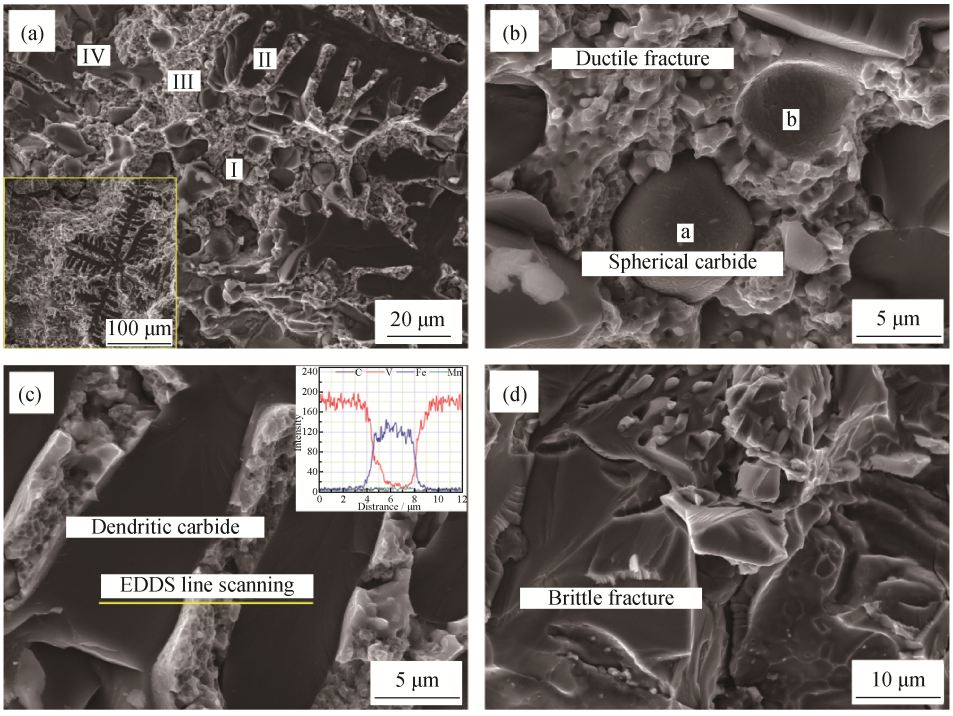

Fig. 6. Fracture morphologies of the 900°C-treated specimen in different regions: (a) different fracture regions; (b) magnified view of ductile fracture and spherical carbide of zone I and zone II in subfigure (a); (c) magnified view of dendritic carbide of zone III in subfigure (a) and EDS composition analysis of line scanning; (d) magnified view of brittle fracture of zone IV in subfigure (a).

impact toughness. In the 1000°C-treated specimen, the carbon diffused from α-Fe to γ-Fe. A higher percentage of γ-Fe (austenite phase) could exist at room temperature because the cooling time was longer than that for the 900°C-treated specimen. The spherical carbide particles of zone I appeared to break but not fall off, as shown in Fig. 7. Therefore, the impact toughness of 1000℃ treated specimen was better than the others with the results of SEM morphology and EDS composition, as shown in Fig. 6 and Fig. 7.

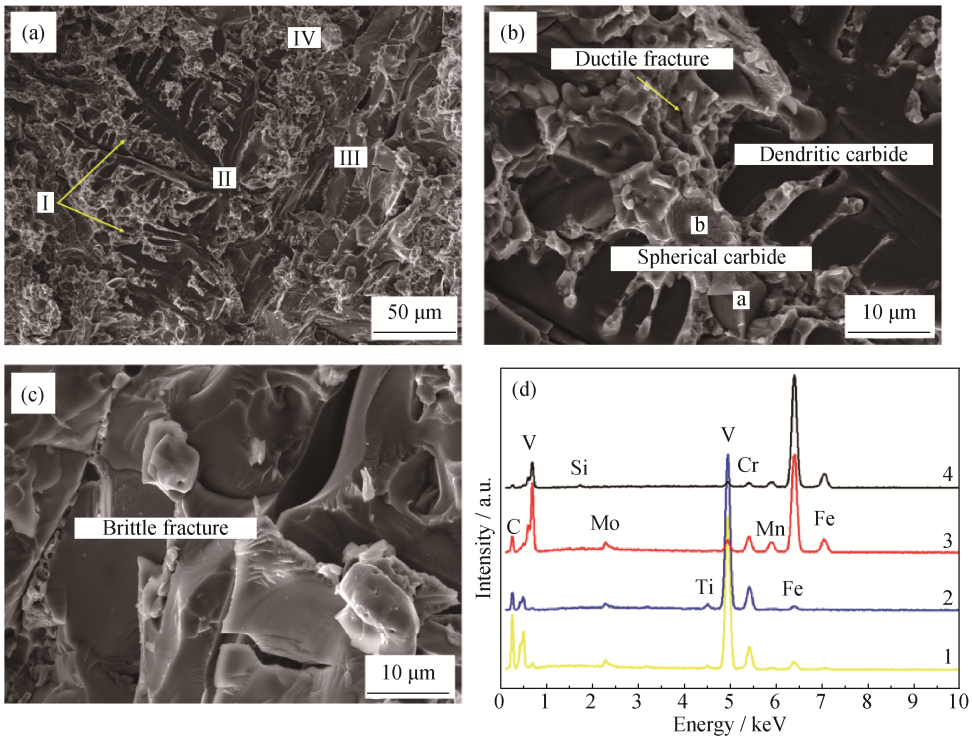

Fig. 7. Fracture morphologies and EDS composition analysis of the 1000°C-treated specimen: (a) showing fracture microstructure for different fracture regions; (b) magnified view of spherical carbides, dendritic carbide and ductile fracture of zone I, zone II and zone IV in (a); (c) magnified view of brittle carbide of zone III in (a); (d) EDS composition analysis of line scanning.

4.2. Effect of heat treatment on wear resistance

Fig. 8 shows the wear morphology of the as-cast (AC), 900°C-treated, and 1000°C-treated specimens. Debris of the YG8 hard alloy was attached to the surface of the AC specimen, whereas a large amount of granular precipitates dispersed in the wear region of the 900°C-treated specimen. Debris of the YG8 hard alloy were detected on the wear surface of the tested specimen austenitized at 1000°C. As shown in Fig. 9, four different types of wear morphologies were characterized by SEM: type 1 (carbide); type 2 (debris of the YG8 hard alloy); type 3 (tested specimen); and type 4 (debris of the tested specimen). Therefore, evaluating whether the specimens treated at different austenitizing temperatures and quenching temperatures exhibited good wear resistance by measuring weight loss was difficult; instead, wear width and depth were taken into account to evaluate the wear resistance, as shown in Fig. 5.

5. Strengthening mechanism

According to previously reported experimental results [15], wear resistance mainly depends on the shape, size, and distribution of vanadium carbide when the microhardness is greater than HRC 58. When the microhardness is less than HRC 58, the wear resistance of the VC-Fe-MCs depends primarily on its hardness and microstructure. Texture of the matrix is almost transformed completely into the austenite texture when the austenitizing temperature is greater than 800°C. Through a rapid quenching treatment, most of the austenite texture is preserved in the matrix. However, the rest can remain in an unstable state. In the subsequent process of carbon partitioning, part of the austenite becomes more stable because of the redistribution of the carbon element. However, the remainder can change from γ-Fe (austenite texture) to α-Fe (martensite texture) during the final cooling process. The microstructure of the Fe-matrix can be transformed

from γ-Fe (good toughness) into α-Fe (excellent hardness and strength) under a certain friction load [27]. The microhardness improves greatly before and after wear test. Different proportions of retained austenite can be achieved through the Q&P process. Therefore, this process and the TRIP effect not only ensure impact toughness but also improve wear resistance during use. On the bases of these experimental results, under friction conditions with either low impact or no impact, an austenitizing temperature of 900°C and a quenching temperature of 180°C are the optimal parameters for improving the microhardness and wear resistance of VC-Fe-MCs. However, under a high-impact condition, an austenitizing temperature of 1000°C and a quenching temperature of 300°C are needed for excellent comprehensive performance.

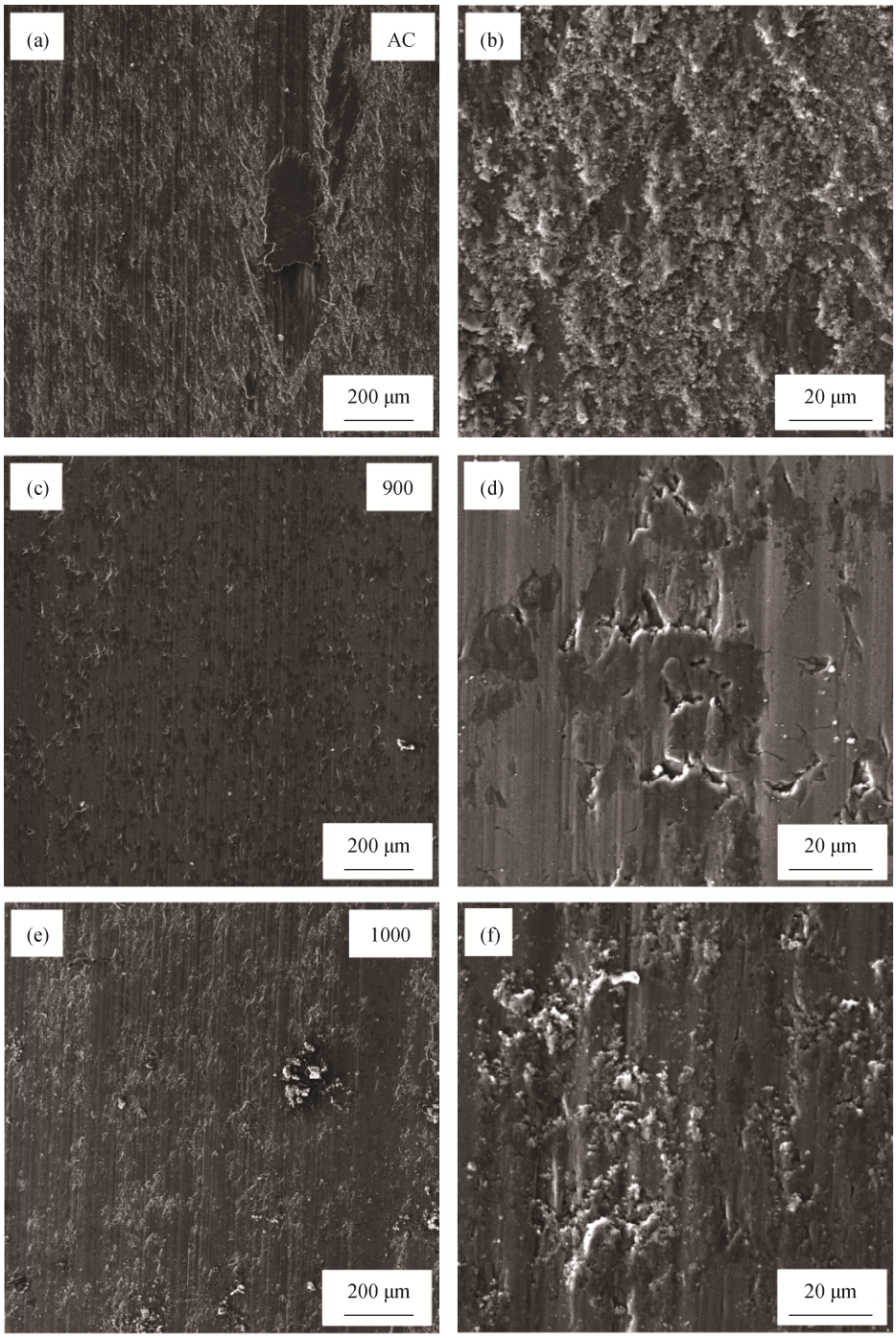

Fig. 8. Wear morphologies of typical specimens: (a) and (b) wear morphologies of an AC specimen; (c) and (d) wear morphologies of a specimen treated at 900°C; (e) and (f) wear morphologies of a specimen treated at 1000°C.

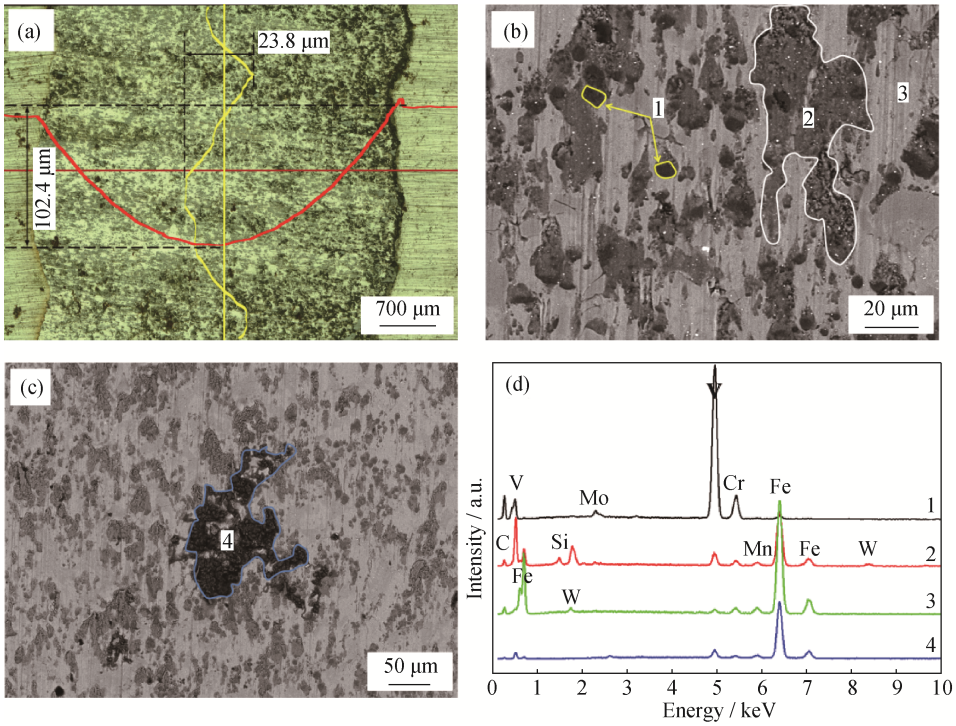

Fig. 9. SEM morphologies (a–c) and EDS analyses (d) of points 1–4 in (b–c) for the 1000°C/300°C-treated specimen after wear test.

6. Conclusions

The microstructure of the Fe-matrix was translated from α-Fe into γ-Fe through a Q&P process, and γ-Fe was stabilized at room temperature through a carbon partitioning treatment. Thus, the TRIP effect was observed because γ-Fe (good toughness) was transformed into α-Fe (excellent hardness and strength) under a certain friction load. In addition, the average hardness was improved substantially before and after wear test. Under low-impact conditions, specimens austenitized at 900°C and quenched at 180°C showed favorable wear resistance; however, under a certain impact condition, the specimens exhibited good wear resistance when austenitized at 1000°C and quenched at 300°C.

Acknowledgements

This work was financially supported by the National Natural Science Foundation of China (Nos. 51475480 and U1637601), the Research Funding from the State Key Laboratory of High-Performance Complex Manufacturing (No. ZZYJKT2017-01), Innovation Platform and Talent Plan of Hunan Province (No. 2016RS2015), and the Project of Innovation Driven Plan in Central South University (No. 2015CX002).

References

[1] L.L. Wu, T.K. Yao, Y.C. Wang, J.W. Zhang, F.R. Xiao, and B. Liao, Understanding the mechanical properties of vanadium carbides: Nano-indentation measurement and first-principles calculations, *J. Alloys Compd.*, 548(2013), p. 60.

[2] B. Zhang and Z.Q. Li, Synthesis of vanadium carbide by mechanical alloying, *J. Alloys Compd.*, 392(2005), No. 1-2, p. 183.

[3] S.V. Shah and N.B. Dahotre, Laser surface-engineered vanadium carbide coating for extended die life, *J. Mater. Process. Technol.*, 124(2002), No. 1-2, p. 105.

[4] H.L. Liu, J.C. Zhu, Y. Liu, and Z.H. Lai, First-principles study on the mechanical properties of vanadium carbides VC and V4C3, *Mater. Lett.*, 62(2008), No. 17-18, p. 3084.

[5] K. Euh, S. Lee, and S. Choo, Microstructural analysis of vanadium carbide/steel surface-alloyed materials fabricated by high-energy electron-beam irradiation, *Metall. Mater. Trans.A.*, 31(2000), No. 11, p. 2849.

[6] G.V. Helden, D. van Heijnsbergen, M.A. Duncan, and G. Meijer, IR-REMPI of vanadium-carbide nanocrystals: Ideal versus truncated lattices, *Chem. Phys. Lett.*, 333(2001), No. 5, p. 350.

[7] H. Zhang, Y. Zou, Z.D. Zou, and W. Zhao, Comparative study on continuous and pulsed wave fiber laser cladding in-situ titanium-vanadium carbides reinforced Fe-based composite layer, *Mater. Lett.*, 139(2015), p. 255.

[8] Y. Wang, Y.C. Ding, W. Jing, F.J. Cheng, and J. Shi, In situ

production of vanadium carbide particulates reinforced iron matrix surface composite by cast-sintering, *Mater. Design*., 28(2007), No. 7, p. 2202.

[9] J.H. Ma, M.N. Wu, Y.H. Du, S.Q. Chen, J. Ye, and L.L. Jin, Low temperature synthesis of vanadium carbide (VC), *Mater. Lett.*, 63(2009), No. 11, p. 905.

[10] H.T. Cao, X.P. Dong, Z. Pan, X.W. Wu, Q.W. Huang, and Y.T. Pei, Surface alloying of high-vanadium high-speed steel on ductile iron using plasma transferred arc alloying technique: Microstructure and wear properties, *Mater. Design*., 100(2016), p. 223.

[11] X.J. Di, M. Li, Z.W. Yang, B.S. Wang, and X.J. Guo, Microstructural evolution, coarsening behavior of vanadium carbide and mechanical properties in the simulated heat-affected zone of modified medium manganese steel, *Mater. Design*., 96(2016), p. 232.

[12] A.G. Rakhshtadt, K.A. Lanskaya, N.M. Suleimanov, and L.V. Katkova, Effect of heat treatment on conditions of formation, shape, and stability of vanadium carbides in vanadium steels, *Met. Sci. Heat Treat.*, 17(1975), No. 6, p. 477.

[13] J. Wang, H. Lu, B. Yu, R.F. Wang, G.M. Hua, X.G. Yan, L. Parent, H. Tian, R. Chung, and D.Y. Li, Explore the electron work function as a promising indicative parameter for supplementary clues towards tailoring of wear-resistant materials, *Mater. Sci. Eng. A*., 669(2016), p. 396.

[14] S.Z. Wei, J.H. Zhu, and L.J. Xu, Research on wear resistance of high speed steel with high vanadium content, *Mater. Sci. Eng. A*., 404(2005), No. 1-2, p. 138.

[15] S.Z. Wei, J.H. Zhu, and L.J. Xu, Effects of vanadium and carbon on microstructures and abrasive wear resistance of high speed steel, *Tribol. Int.*, 39(2006), No. 7, p. 641.

[16] L.S. Zhong, F.X. Ye, Y.H. Xu, and J.S. Li, Microstructure and abrasive wear characteristics of in situ vanadium carbide particulate-reinforced iron matrix composites, *Mater. Design*., 54(2014), p. 564.

[17] S. Yan, X.H. Liu, W.J. Liu, H.F. Lan, and H.Y. Wu, Comparison on mechanical properties and microstructure of a C-Mn-Si steel treated by quenching and partitioning (Q&P) and quenching and tempering (Q&T) processes, *Mater. Sci. Eng. A*., 620(2015), p. 58.

[18] G.H. Gao, B.F. An, H. Zhang, H.R. Guo, X.L. Gui, and B. Bai, Concurrent enhancement of ductility and toughness in an ultrahigh strength lean alloy steel treated by bainite-based quenching-partitioning-tempering process, *Mater. Sci. Eng. A*., 702(2017), p. 104.

[19] S. Boettcher, M. Böhm, and M. Wolff, Well-posedness of a thermo-elasto-plastic problem with phase transitions in TRIP steels under mixed boundary conditions, *ZAMM-Z. Angew. Math. Me.*, 95(2016), No. 12, p. 1461.

[20] A. Ramazani, H. Quade, M. Abbasi, and U. Prahl, The effect of martensite banding on the mechanical properties and formability of TRIP steels, *Mater. Sci. Eng. A*., 651(2016), p. 160.

[21] L. Luo, W. Li, L. Wang, S. Zhou, and X. Jin, Tensile behaviors and deformation mechanism of a medium Mn-TRIP steel at different temperatures, *Mater. Sci. Eng. A*., 682(2016), p. 698.

[22] Z.C. Li, H. Ding, R.D.K. Misra, and Z.H. Cai, Microstructure-mechanical property relationship and austenite stability in medium-Mn TRIP steels: The effect of austenite-reverted transformation and quenching-tempering treatments, *Mater. Sci. Eng. A*., 682(2017), p. 211.

[23] P.J. Jacques, Q. Furnémont, F. Lani, T. Pardoen, and F. Delannay, Multiscale mechanics of TRIP-assisted multiphase steels: I. Characterization and mechanical testing, *Acta Mater.*, 55(2007), No. 11, p. 3681.

[24] Z.C. Li, H. Ding, R.D.K. Misra, Z.H. Cai, and H.X. Li, Microstructural evolution and deformation behavior in the Fe-(6, 8.5)Mn-3Al-0.2C TRIP steels, *Mater. Sci. Eng. A*., 672(2016), p. 161.

[25] J.P. Zhou, K. Shimizu, and Q.Z. Cai, Effects of Cr content and annealing temperature on microstructure and wear characteristics of cast ausferrite nodular iron, *J. Iron. Steel Res. Int.*, 22(2015), No. 11, p. 1049.

[26] X.Y. Chong, Y.H. Jiang, R. Zhou, and J. Feng, The effects of ordered carbon vacancies on stability and thermo-mechanical properties of V_8C_7 compared with VC, *Sci. Rep.*, 6(2016), p. 34007.

[27] J.M. Torralba, A. Navarro, and M. Campos, From the TRIP effect and Quenching and Partitioning steels concepts to the development of new high-performance, lean powder metallurgy steels, *Mater. Sci. Eng. A*., 573(2013), p. 253.